nature COMMUNICATIONS

ARTICLE

Received 20 Jul 2015 | Accepted 22 Jan 2016 | Published 4 Mar 2016

DOI: 10.1038/ncomms10819 OPEN

# Commensurate antiferromagnetic excitations as a signature of the pseudogap in the tetragonal high-$T_c$ cuprate $HgBa_2CuO_{4+\delta}$

M.K. Chan[1,2], C.J. Dorow[1,†], L. Mangin-Thro[3], Y. Tang[1], Y. Ge[1,†], M.J. Veit[1,†], G. Yu[1], X. Zhao[1,4], A.D. Christianson[5], J.T. Park[6], Y. Sidis[3], P. Steffens[7], D.L. Abernathy[5], P. Bourges[3] & M. Greven[1]

Antiferromagnetic correlations have been argued to be the cause of the *d*-wave superconductivity and the pseudogap phenomena exhibited by the cuprates. Although the antiferromagnetic response in the pseudogap state has been reported for a number of compounds, there exists no information for structurally simple $HgBa_2CuO_{4+\delta}$. Here we report neutron-scattering results for $HgBa_2CuO_{4+\delta}$ (superconducting transition temperature $T_c \approx 71$ K, pseudogap temperature $T^* \approx 305$ K) that demonstrate the absence of the two most prominent features of the magnetic excitation spectrum of the cuprates: the X-shaped 'hourglass' response and the resonance mode in the superconducting state. Instead, the response is Y-shaped, gapped and significantly enhanced below $T^*$, and hence a prominent signature of the pseudogap state.

[1] School of Physics and Astronomy, University of Minnesota, Minneapolis, Minnesota 55455, USA. [2] Pulsed Field Facility, National High Magnetic Field Laboratory, Los Alamos National Laboratory, Los Alamos, New Mexico 87545, USA. [3] Laboratoire Léon Brillouin, LLB/IRAMIS, UMR12, CEA-CNRS, CEA-Saclay, Gif sur Yvette 91191, France. [4] State Key Lab of Inorganic Synthesis and Preparative Chemistry, College of Chemistry, Jilin University, Changchun 130012, China. [5] Quantum Condensed Matter Division, Oak Ridge National Laboratory, Oak Ridge, Tennessee 37831, USA. [6] Forschungsneutronenquelle Heinz Maier-Leibnitz, Garching 85747, Germany. [7] Institute Laue Langevin, Grenoble 38042 CEDEX 9, France. † Present address: Department of Physics, University of California, San Diego, 9500 Gilman Drive La Jolla, California 92093, USA (C.J.D.); Department of Physics, Penn State University, University Park, Pennsylvania 16802, USA (Y.G.); Department of Applied Physics, Stanford University, Stanford, California 94305, USA (M.J.V.). Correspondence and requests for materials should be addressed to M.K.C. (email: mkchan@lanl.gov) or to M.G. (email: greven@physics.umn.edu).

Most of the detailed knowledge about magnetic fluctuations in the cuprates comes from neutron-scattering studies of $La_{2-x}Sr_xCuO_4$ (LSCO) and $YBa_2Cu_3O_{6+y}$ (YBCO)[1,2]. The momentum ($\mathbf{Q}$) and energy- ($\omega$) dependent dynamic magnetic susceptibility $\chi''(\mathbf{Q},\omega)$ of LSCO is characterized by an X-shaped hourglass spectrum that disperses with increasing energy from incommensurate wave vectors at $\omega \approx 0$ towards the antiferromagnetic wave vector $\mathbf{q}_{AF}$, and then outward again at higher energies[1,3]. YBCO exhibits a similar dispersion in the superconducting (SC) state, yet its foremost characteristic is the magnetic resonance, a large and abrupt susceptibility increase at $\mathbf{q}_{AF}$ and a well-defined energy $\omega_r$ upon cooling below $T_c$ (ref. 2). Despite the apparent ubiquity of the hourglass dispersion, the differences between the spectra for LSCO and YBCO have motivated ostensibly contradictory microscopic interpretations: incommensurate spin-density-wave (SDW) fluctuations of local moments (unidirectional charge-spin stripe order is one example)[4], or a spin-exciton because of particle–hole excitations in the SC state[2,5]. The persistence of low-energy incommensurate excitations at temperatures well above $T_c$ for both LSCO and YBCO has stimulated speculation that the opening of the pseudogap (PG) is associated with SC[6] or SDW[1,7,8] fluctuations.

Although it has long been known that AF correlations may cause the $d$-wave superconductivity exhibited by the cuprates[9], such theoretical approaches were not thought to be able to account for the PG phenomenology. Following recent theoretical advancements[10], it has been argued that AF correlations may not only drive $d$-wave superconductivity, but potentially also PG electronic instabilities such as charge order (charge-density-wave (CDW), bond-density-wave), translational symmetry-preserving ($\mathbf{q}=0$) loop-current order, and pair-density-wave order[11–14]. These developments raise the prospect that much of the cuprate phase diagram may be understood as driven by AF correlations. It is therefore imperative to determine the detailed magnetic response in a structurally simple compound in which both CDW[15] and $\mathbf{q}=0$ (refs 16,17) order have been firmly established. Such measurements might also help illuminate the relevance of the seemingly universal hourglass response.

$HgBa_2CuO_{4+\delta}$ (Hg1201) features the highest optimal $T_c$ ($T_{c,max}=97$ K) of the single-$CuO_2$-layer cuprates (for example, $T_{c,max}=39$ K for LSCO; YBCO has $T_{c,max}=93$ K and a double-$CuO_2$-layer structure), a simple tetragonal crystal structure, and minimal disorder effects[18]. Similar to the recent demonstration of the validity of Kohler's rule for the magnetoresistance in the PG phase[19], these model-system characteristics of Hg1201 can be expected to most clearly reveal the inherent magnetic fluctuation spectrum of the quintessential $CuO_2$ layers.

We present an inelastic neutron-scattering study of the magnetic excitations of an underdoped Hg1201 sample with $T_c \approx 71$ K and hole doping $p \approx 0.095$ (labelled HgUD71; see Methods, Supplementary Notes 1–2 and Supplementary Figs 1–5 for detailed experimental and analysis information). This is a particularly interesting doping level because it corresponds to the shoulder of the 'SC dome', where $T_c$ appears to be slightly suppressed, and because a cascade of phenomena have been observed: quasi-static $\mathbf{q}=0$ magnetic order[16,17] below $T^*$, short-range CDW correlations[15] below $T_{CDW} \approx 200$ K, evidence for Fermi-liquid transport in the PG state[19–21], and Shubnikov-de Haas oscillations (below 4 K in magnetic fields above 60 T) (ref. 22). The slight suppression of $T_c$ at this doping level might be a signature of a competing ground state, and it is interesting to determine if this has an effect on the dynamic magnetic susceptibility. As shown in Fig. 1a, the situation for Hg1201 mirrors the phenomenology of underdoped YBCO[23–28]. We find that the dynamic magnetic response of HgUD71 is characterized by a gapped Y-shaped dispersion that is commensurate with $\mathbf{q}_{AF}$ at energies below about 60 meV. Interestingly, the magnetic scattering exhibits a marked increase below the PG temperature $T^*$ yet is largely impervious to the onset of CDW order and of superconductivity. This establishes the commensurate excitations as a signature of the PG state.

## Results

**Time-of-flight neutron spectroscopy**. Figures 2a,b shows $\chi''(\mathbf{Q},\omega)$ at 5 and 85 K for HgUD71 extracted from raw neutron-scattering data. At 5 K, deep in the SC phase, the susceptibility exhibits a prominent peak at $\omega_{peak} \approx 51$ meV and is gapped below $\Delta_{AF} \approx 27$ meV (see Supplementary Notes 3 and Supplementary Fig. 6 for limits on the low-energy scattering). Up to approximately $\omega_{com}=59$ meV, the response is commensurate with $\mathbf{q}_{AF}$, and then it disperses outward at higher energies, resulting in a gapped Y-shaped spectrum (Figs 2a,c–g,3e). The magnetic nature of the response is confirmed through spin-polarized neutron scattering and also from its $\mathbf{Q}$ dependence, which follows the magnetic form factor (see Supplementary Notes 4 and Supplementary Fig. 7).

We fit constant-$\mathbf{Q}$ data such as those in Fig. 2c–l to a Gaussian form, $\chi''(\mathbf{Q},\omega)=\chi_0''\exp\{-4\ln 2R/(2\kappa)^2\}$, convolved with the momentum resolution of the instrument (Supplementary Fig. 2), where $R=|[(H\text{-}1/2)^2+(K\text{-}1/2)^2]^{1/2}\text{-}\delta|^2$, $2\kappa$ is the full-width at half-maximum (FWHM), and $\delta$ parameterizes the incommensurability away from $\mathbf{q}_{AF}$. The energy dependences of $\chi_0''$, $2\kappa$ and $\delta$ are shown in Fig. 3a,b inset, and Fig. 3e, respectively.

**Commensurate low-energy magnetic excitations**. As shown in Fig. 2, the low-energy magnetic excitations in HgUD71 are commensurate with $\mathbf{q}_{AF}$. In Fig. 3e, $\delta=0$ for $\omega<\omega_{com}$, since this results in the best fit to the data. We also fit the data with $\delta\neq 0$ (Fig. 4a) to facilitate comparison with published results for YBCO and LSCO (Fig. 4b,c), where at the neck of the hourglass a non-zero value of $\delta$ is typically employed in the data analysis even when the response is essentially commensurate. We find an upper bound of $\delta \approx 0.03$ r.l.u. for HgUD71 ($\omega<\omega_{com}$), which is consistent with the half-width at half-maximum of the instrumental momentum resolution (Fig. 4a and Supplementary Fig. 2). As seen from Fig. 4b,c, this upper bound is significantly smaller than the incommensurability observed in both LSCO and YBCO at similar doping levels.

**Evolution of magnetic excitations across $T^*$ and $T_c$**. Figure 3a shows the energy dependence of the susceptibility amplitude $\chi_0''$ at four temperatures. A comparison of the data at 5 and 85 K reveals hardly any effect of superconductivity. This is also apparent from Fig. 3c, which shows the change $\Delta\chi_0''$ between these two temperatures. As seen from Fig. 3a, a further increase of temperature suppresses $\chi_0''$ at all measured energies (up to 53 meV for $T>85$ K).

To better ascertain the temperature dependence of magnetic excitations, we focus on the response at $\omega_{peak} \approx 51$ meV and $\mathbf{q}_{AF}$ (Fig. 1b). Consistent with Fig. 3a, the intensity does not exhibit an abrupt change across $T_c$, which confirms the lack of a magnetic resonance. However, a marked increase in intensity occurs below the PG temperature $T^*$. For comparison, we measured the temperature dependence of the intensity of the odd-parity resonance mode of YBCO at a similar doping level (sample labelled YBCO6.6: $y=0.6$, $T_c=61$ K, $p=0.11$ and $\omega_r=32$ meV; see black arrow in Fig. 1a). The result is shown in Fig. 1c. As for HgUD71, the intensity for YBCO6.6 increases below $T^*$, yet in contrast to HgUD71, a large magnetic resonance is observed below $T_c$.

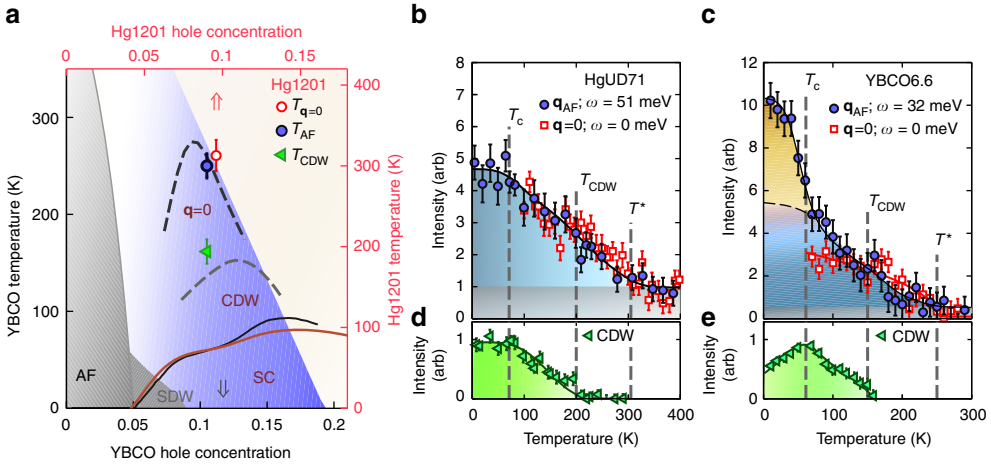


**Figure 1 | Phase diagram of Hg1201 and YBCO.** (**a**) Phase diagram: Hg1201 (red top-right axes) and YBCO (black bottom-left axes). The axes are adjusted such that the $T_c(p)$ domes of Hg1201 (red line) and YBCO (black line) approximately line up. The blue region represents the PG regime. The red and grey arrows indicate the doping of HgUD71 ($T_c = 71$ K) and YBCO6.6 ($T_c = 61$ K) highlighted in this work. Dashed black and grey lines represent the temperatures below which $\mathbf{q} = 0$ magnetic order[23,24] and CDW[25–27] correlations are observed in YBCO. The corresponding data for Hg1201 ($T_{\mathbf{q}=0}$, red circle; $T_{CDW}$, green triangle) for doping levels close to HgUD71 are shown[15–17]. The significant increase in the AF response appears below $T_{AF}$ (blue circle). Grey shaded and hashed areas represent AF and SDW[28] order in YBCO. (**b**) Temperature dependence of inelastic magnetic scattering at $\mathbf{q}_{AF}$ and $\omega_{peak} = 51$ meV and of quasi-elastic (FWHM energy resolution ~1 meV) magnetic scattering at $\mathbf{q} = 0$ (from ref. 17) measured on separate Hg1201 samples with similar doping levels ($T_c = 71$ and 75 K, respectively). We determine $T_{\mathbf{q}=0} = 320 \pm 20$ K (ref. 17) and $T_{AF} = 300 \pm 15$ K. The $\mathbf{q} = 0$ signal is shifted upward (by one unit) for comparison. Both $T_{\mathbf{q}=0}$ and $T_{AF}$ are consistent with $T^* = 305 \pm 10$ K determined from the planar resistivity (deviation from high-temperature linear dependence)[19]. (**c**) Temperature dependence of the $\mathbf{q} = 0$ signal[23] and of the odd-parity resonance ($\omega_r = 32$ meV) for a twinned YBCO6.6 sample (see Methods for sample details). For **b**,**c**, the blue region represents the increase in intensity in the PG state and the grey region is the baseline intensity for $T > T^*$. The shaded orange region in **c** represents the excess scattering below $T_c$ because of the resonance mode. (**d**,**e**) Temperature dependence of short-range CDW order in Hg1201 (ref. 15) and YBCO (ref. 26) at approximately the same respective doping levels as the data in **b**,**c**. Vertical error bars in **a**–**c** are statistical errors (1 s.d.).

Even though HgUD71 does not exhibit a magnetic resonance, upon cooling into the SC phase we observe subtle changes in the susceptibility at wave vectors away from $\mathbf{q}_{AF}$ and at energies below and above $\omega_{peak}$, centred at $\omega_1 = 44$ meV and $\omega_2 = 75$ meV. This is best seen from the momentum-integrated local susceptibility, $\chi''_{loc}(\omega) = \int \chi''(\mathbf{Q},\omega) d^2q / \int d^2q$ (Fig. 3b,d). At $\omega_1$, the change across $T_c$ ($\Delta\chi''_{loc}$) is due to a slight increase of both the momentum width and intensity, whereas at $\omega_2$ it results from an increase in amplitude on the upward dispersive part of the spectrum (see also Fig. 2c,h,m). The **Q** dependence of these subtle changes across $T_c$ is discussed in more detail in Supplementary Note 5 and Supplementary Fig. 8.

## Discussion

The absence of an hourglass dispersion in HgUD71 constitutes a clear departure from the purported universal magnetic response of the cuprates. Figure 4 compares the **Q**-$\omega$ dispersion of the magnetic fluctuations centred at $\mathbf{q}_{AF}$ at similar doping levels for HgUD71, YBCO6.6 (refs 7,8) and LSCO ($p \approx 0.085$, $T_c = 22$ K)[3]; see Supplementary Fig. 9 for an additional comparison between HgUD71 and LSCO ($p \approx 0.085$). LSCO exhibits a gapless hourglass dispersion both in the SC state and in the normal state. In the local moment picture, the incommensurate low-energy response is argued to be a signature of SDW correlations[1]. For underdoped LSCO[1] and YBCO[28], the occurrence of incommensurate SDW order revealed by neutron-scattering correlates with a planar resistivity characterized by a sizable extrapolated zero-temperature residual and by a low-temperature insulating-like upturn (when superconductivity is suppressed with large magnetic fields) below a non-universal critical doping $p_c$; $p_c \approx 0.16$ for LSCO[29] and $p_c \approx 0.085$ YBCO[30]. The doping-temperature range of the SDW correlations in YBCO is shown in Fig. 1a. At the doping level of our study, Hg1201 exhibits electrical transport without a significant zero-temperature residual[20], Kohler scaling of the normal state magneto-resistance[19], as well as quantum oscillations[22], which demonstrates an underlying metallic ground state. Although $p_c$ for Hg1201 is not known, it is likely smaller than $p \approx 0.055$ ($T_c = 45$ K), for which the residual resistivity is still very small[20]. In addition to the commensurate low-energy response reported here for HgUD71, this indicates that Hg1201 is less prone to SDW order than YBCO and especially LSCO.

In the SC state, YBCO[7] (for $p > p_c$) exhibits a prominent resonance and a gapped magnetic response that is hourglass-shaped (Figs 1c,4b). The hourglass dispersion and resonance are best explained as signatures of the *d*-wave SC order parameter within the itinerant spin-exciton picture[2,5]. Although the resonance is well established over a wide doping range in double-layer YBCO[2], for single-layer compounds ($Tl_2Ba_2CuO_{6+\delta}$ (ref. 2) and Hg1201 (ref. 31)) it has been reported only close to optimal doping, where the PG phenomenon is less prominent. According to the relationship $\omega_r/2\Delta_{SC} = 0.64 \pm 0.04$ found for unconventional superconductors[32], and with the estimate $2\Delta_{SC} = 78$–$91$ meV from electronic Raman scattering[33] and photoemission spectroscopy[34], we expect $\omega_r \approx 54$ meV, which is close to $\omega_{peak} \approx 51$ meV for HgUD71. Interpreted within the spin-exciton picture, the suppression of the magnetic resonance at $\mathbf{q}_{AF}$ might result from an absence of coherent Bogoliubov quasi-particles at the 'hotspots' (where the underlying Fermi surface intersects the AF Brillouin zone boundary) as a result of the antinodal PG. This is consistent with electronic Raman scattering for Hg1201 (refs 33,35), namely the fact that the SC pair-breaking peak in the $B_{1g}$ channel, which probes the antinodal states, significantly weakens upon underdoping (samples with $T_c$ below about 78 K), whereas

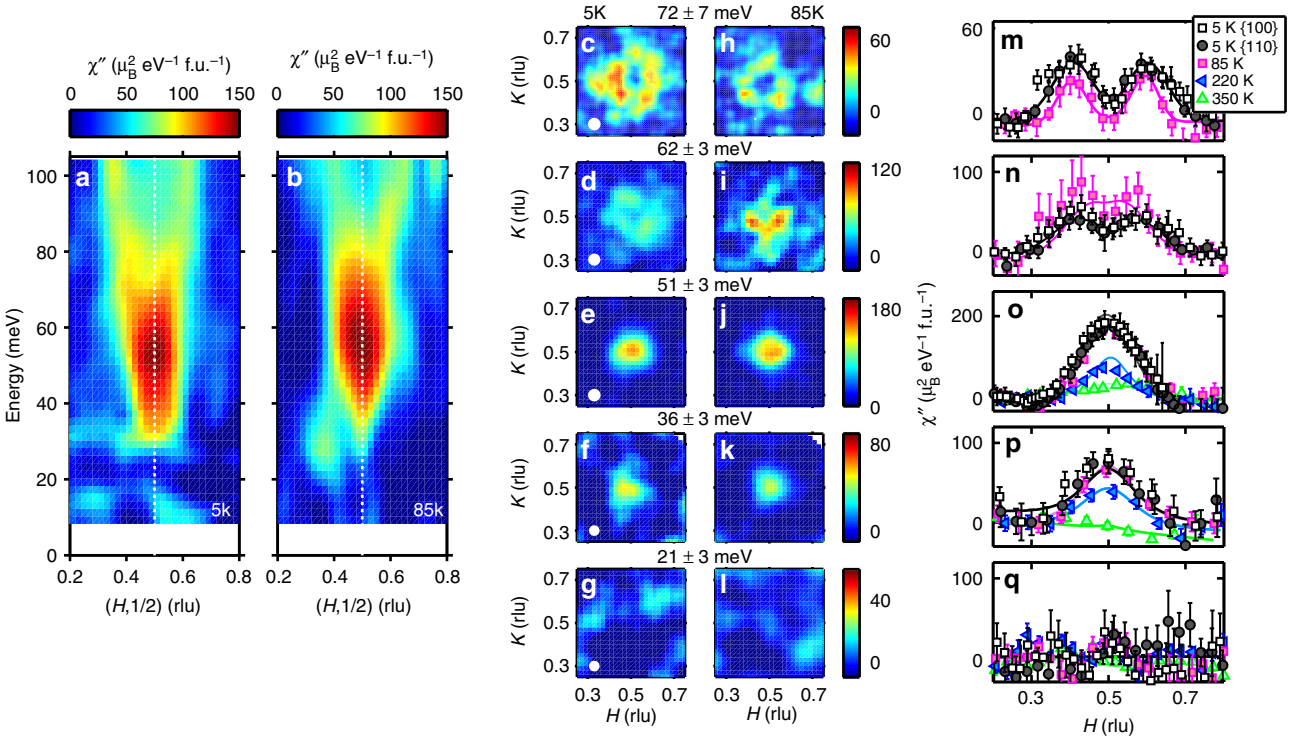


**Figure 2 | Magnetic excitation spectrum of HgUD71 features gapped, commensurate and dispersive components.** (**a**,**b**) Energy dependence of $\chi''(\mathbf{Q},\omega)$ for HgUD71 at 5 and 85 K (14 K above $T_c$), respectively, along the two-dimensional momentum-transfer trajectory [*H*,0.5], with intensity averaged over the range $K = 0.5 \pm 0.12$. The gap $\Delta_{AF}$ is defined as the energy below which no scattering is observed at $\mathbf{q}_{AF}$; $\Delta_{AF} \approx 27$ meV at both 5 and 85 K. (**c**–**l**) Constant-energy slices of magnetic scattering at $T = 5$ K in **c**–**g** and $T = 85$ K in **h**–**l**. (**m**–**q**) The corresponding constant-energy cuts along high-symmetry trajectories. Cuts along {100} (average of [H00] and [0H0] cuts) and {110} (average of [HH0] and [H-H0] cuts) are shown for $T = 5$ K (open black squares and closed black circles, respectively). Data at higher temperatures (85, 220 and 350 K) are averages of four cuts along [H00], [0H0], [HH0] and [H-H0] trajectories. Error bars represent statistical error (1 s.d.). The white circles in **c**–**g** represent the momentum resolution at the corresponding energy transfers. Data collected on ARCS (see Methods).

the peak in the $B_{2g}$ channel, which probes the nodal states, persists. It is furthermore consistent with our observation of an increase of $\chi''(\mathbf{Q},\omega)$ below $T_c$ at momenta away from $\mathbf{q}_{AF}$ that connect parts of the Fermi-surface closer to the coherent nodal directions that are unaffected by the PG.

The significant increase of the magnetic response below $T^*$ (Fig. 1b) and the concomitant absence of a prominent effect across $T_c$ indicates that the AF response for HgUD71 is dominated by the PG formation. The latter is a pivotal characteristic of the cuprates, and it is possibly associated with an underlying quantum critical point that controls much of the phase diagram[36,37]. A close connection between $\chi''(\mathbf{Q},\omega)$ and the PG has been suggested before[3,6,7]. In early work on YBCO, it was argued that the magnetic fluctuations in the PG state are a precursor of the resonance and therefore a signature of fluctuating superconductivity[6]. However, more recent work[7] on detwinned YBCO6.6 found that $\chi''(\mathbf{Q},\omega)$ in the PG state is in fact distinct from that in the SC state. Furthermore, the broken fourfold structural symmetry of YBCO results in a large anisotropy in $\chi''(\mathbf{Q},\omega)$ for the two in-equivalent planar crystallographic directions. Whereas the dispersion along [010] is reminiscent of the commensurate Y-shaped spectrum of HgUD71, the response along [100] is broader and incommensurate at low energies (Fig. 4c) (ref. 7). This led to speculation that the PG is characterized either by stripe fluctuations, similar to LSCO, or by a nematic instability[7]. However, an alternative explanation for the anisotropy is interlayer coupling to the unidirectional CuO chain states of YBCO[38], a complication that is absent in HgUD71. Our result for this structurally simpler cuprate, showing a PG state characterized by a commensurate and isotropic low-energy magnetic response with no connection to a magnetic resonance, calls for a new theoretical interpretation. We speculate that the commensurate response for $\omega < \omega_{com}$ predominantly results from particle–hole scattering near the AF hotspots, and that it involves the non-dispersive region in the spectral density of states determined from scanning tunnelling microscopy in the PG state[39].

A number of broken symmetries have been identified in the PG regime. In particular, the cuprates exhibit strong ($\sim 0.1\ \mu_B$) $\mathbf{q} = 0$ quasi-elastic magnetism[16,17,23,24] that is qualitatively consistent with intra-unit-cell loop-current order[37]. We demonstrate in Fig. 1b that the significant enhancement of fluctuations at $\mathbf{q}_{AF}$ coincides with the onset of $\mathbf{q} = 0$ magnetism for HgUD71, which establishes a connection between these two seemingly distinct magnetic phenomena and with the opening of the PG at $T^*$. On the other hand, (short-range) CDW correlations first appear at a temperature that is distinctly lower than $T^*$ (ref. 15) and have no discernible effect on the magnetic fluctuations (Fig. 1b,d, Supplementary Notes 6, Supplementary Fig. 10). Regarding the changes across $T^*$, our result suggests that the development of AF correlations is a consequence rather than the cause of the PG. Nevertheless, these correlations might drive the subsequent CDW order, which in turn drives the Fermi-surface reconstruction implied by transport experiments in high magnetic fields[15,22,30]. It will be important to assess if this can indeed be the case given an instantaneous magnetic correlation length (estimated from integration over the measured energy range) of about two to three lattice constants in HgUD71.

Figure 1b–e show that, similar to HgUD71, for YBCO6.6 the intensity of the response at $\mathbf{q}_{AF}$ increases substantially along with the onset of $\mathbf{q} = 0$ order at $T^*$. In contrast to HgUD71, for

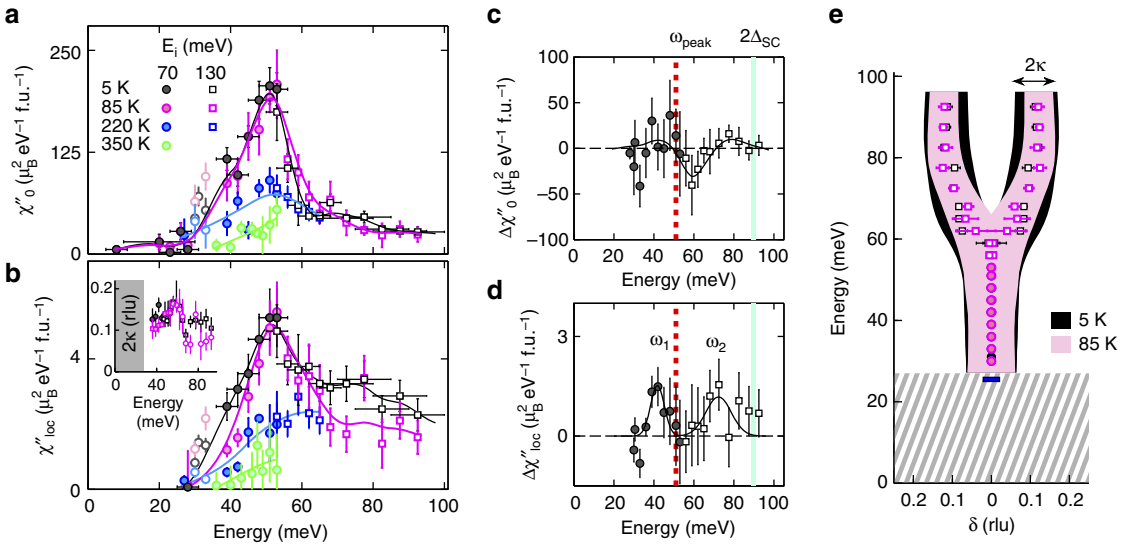


**Figure 3 | Magnetic susceptibility amplitude and local susceptibility for HgUD71.** (**a**) Energy dependence of the measured peak magnetic susceptibility $\chi''_0$ at $T=300$, 220, 85 and 5 K. Closed circles: $E_i=70$ meV. Open squares: $E_i=130$ meV. Solid lines: guides to the eye. Horizontal bars for the 5 K data represent energy bins. The same binning is used at higher temperatures. Between 30 and 33 meV the data are systematically contaminated by aluminium and phonon scattering, and are represented as lighter open symbols (see Supplementary Fig. 3). (**b**) Same legend as **a**. Energy dependence of the momentum-integrated (local) susceptibility $\chi''_{loc}$. In determining $\chi''_{loc}$, we assume that AF fluctuations are quasi-two-dimensional, that is, that $\chi''$ does not depend on $L$. Inset: $2\kappa$ (FWHM) as a function of energy at 5 K (black) and 85 K (magenta). (**c**,**d**) Change of $\chi''_0$ and $\chi''_{loc}$, respectively, between 5 and 85 K (that is, across $T_c$). Filled and open symbols: $E_i=70$ and 130 meV, respectively. The red vertical line marks $\omega_{peak}$. The turquoise line represents $2\Delta_{SC}$, where $\Delta_{SC}=45\pm1$ meV is the maximum SC $d$-wave gap determined from Raman scattering[33]. Black line in **c**: guide to the eye. Black line in **d**: fit to two Gaussian peaks, located at $\omega_1=44\pm2$ meV and $\omega_2=75\pm2$ meV. (**e**) Energy dependence of incommensurability $\delta$ at 5 K (black) and 85 K (red). Horizontal error bars are fit uncertainties for $\delta$. For $\omega<59$ meV, the data are best described with $\delta=0$. We estimate an upper bound of $\delta\approx0.03$, which is the approximate value of the instrumental momentum resolution in the $\omega=27$–59 meV range. Shaded black and magenta regions represent $2\kappa$ at 5 and 85 K, respectively. Hatched area indicates the gap $\Delta_{AF}$. Horizontal blue bar at $\omega=27$ meV represents the instrumental momentum resolution at that energy for $E_i=70$ meV. All vertical error bars in figure are least-square fit errors (1 s.d.).

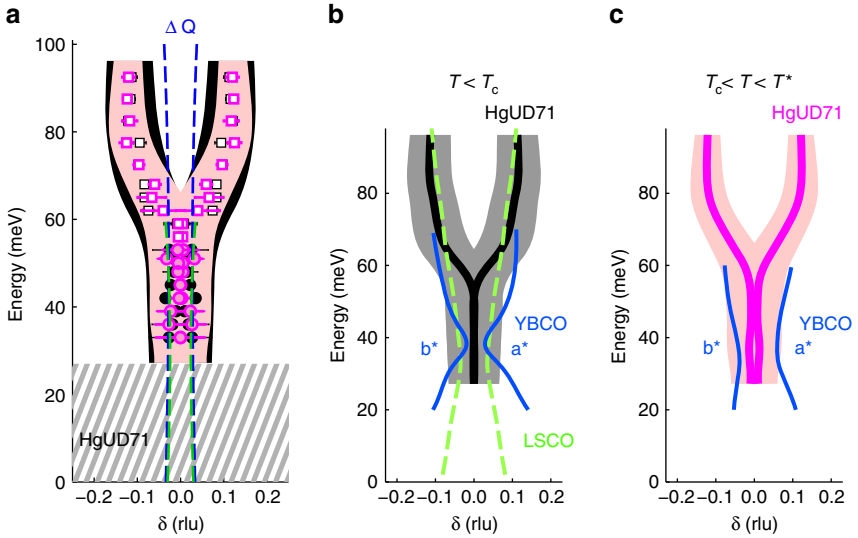


**Figure 4 | Comparison of Y-shaped response of HgUD71 with magnetic excitation spectrum of YBCO and LSCO at similar doping levels.** (**a**) Energy dependence of incommensurability $\delta$ at 5 K (black) and 85 K (magenta), with $\delta$ assumed to be non-zero at all energies. We arrive at an upper bound of $\delta\sim0.03$ r.l.u., which corresponds to the half-width at half-maximum of the instrumental **Q** resolution (FWHM resolution for $E_i=70$ and 130 meV indicated by the green and blue dotted lines, respectively). Shaded black and red regions represent the measured FWHM ($2\kappa$) at 5 and 85 K, respectively. Hatched grey area indicates the gap in the excitation spectrum. (**b**) Comparison of the dispersion of HgUD71 with YBCO6.6 (ref. 7,8) and LSCO ($p=x=0.085$) (ref. 3) deep in the SC state. (**c**) Comparison of the dispersion of HgUD71 with YBCO6.6 above $T_c$ ($T=85$ and 70 K, respectively)[7]. The response of orthorhombic YBCO6.6 (blue lines) is anisotropic, and therefore $\delta$ along both a* (right) and b* (left) is shown. As in **a**, the shaded regions in **b**,**c** indicate the momentum widths (FWHM) of the response of HgUD71.

YBCO6.6 this is followed by a large resonance below $T_c$ and by the concomitant appearance of the low-energy hourglass structure[7,8] and of a significant suppression of the CDW response[26]. This indicates differing relative strengths of the SC and PG order parameters at temperatures below $T_c$ for the two cuprates.

In summary, the AF response of the underdoped cuprates can be divided into three distinct types: (1) the gapless X-shaped spectrum associated with incommensurate SDW correlations of local moments in the La-based compounds[1] and in lightly doped YBCO[28], where $\mathbf{q}=0$ magnetism is suppressed because of the competing SDW instability[24]; (2) the gapped X-shaped spectrum and magnetic resonance attributed to particle–hole excitations in the SC state[2,5]; and (3) the gapped Y-shaped spectrum associated with the PG formation (and with $\mathbf{q}=0$ magnetism[16,17] and metallic charge transport[19,20,22]) revealed most clearly in tetragonal Hg1201. The balance between PG, SDW and SC order parameters determines the magnetic response for a particular compound, doping level and temperature. We note that similar to LSCO, single-layer $Bi_{2+x}Sr_{2-x}CuO_{6+y}$ (Bi2201) exhibits a propensity towards SDW order[40], whereas double-layer $Bi_2Sr_2CaCu_2O_{8+\delta}$ (Bi2212) near optimal doping features a dispersive resonance reminiscent of YBCO[41]. Just as for LSCO, $T_{c,max}=38$ K (ref. 18) for Bi2201 is relatively low. Interestingly, the magnetic response of single-layer Hg1201 more closely resembles that of double-layer YBCO than those of single-layer LSCO and Bi2201. Yet the dominant PG behaviour is most clearly apparent in Hg1201, which does not feature the complications of YBCO because of the orthorhombic double-layer structure (even vs odd-parity magnetic excitations; in-equivalent response along [100] and [010]). To build a connection with the distinct magnetic response of the low-$T_{c,max}$ single-layer compounds LSCO and Bi2201, it might be necessary to study Hg1201 with intentionally introduced disorder. Furthermore, experiments on Hg1201 at lower doping levels will be necessary to ascertain if the SDW instability is in fact a universal property of the cuprates.

## Methods

**Sample preparation.** Single crystals of $HgBa_2CuO_{4+\delta}$ were grown by a two-step self-flux method[42]. As-grown crystals are typically underdoped, with $T_c\approx81$ K. To reach the desired doping level, the crystals were annealed at 400 °C in a partial vacuum of 100 mtorr for 80 days[43]. The SC transition temperature of the individual crystals was subsequently determined from measurements of the Meissner effect in a SQUID magnetometer: each crystal was cooled in zero magnetic field, and the susceptibility was monitored upon warming in a 5 Oe field applied along the crystallographic $c$ axis. Supplementary Fig. 1 shows the average susceptibility of all the 34 crystals that made up the HgUD71 sample. We find $T_c\approx71$ K (defined as the midpoint of the transition) with a full transition width of $\Delta T_c=5$ K for the assembled sample, and estimate $p\approx0.095$ based on our thermoelectric power measurements of crystals from the same annealing batches. The doping level we estimate from these measurements is 0.005 higher than that estimated from prior published values for powder samples with the same $T_c$ (ref. 44). The rather narrow combined transition width indicates a high degree of homogeneity and quality of the sample. We note that smaller crystals from the same growth and annealing batches exhibit Shubnikov-de Hass oscillations[22]. The fact that quantum oscillations can be observed at low temperatures is a consequence of the very small residual resistivity exhibited by these crystals[20]. The 34 crystals, with masses ranging from $\sim$20 to 125 mg, were polished parallel to the $ab$-plane and co-aligned on two aluminium plates with GE-varnish using a Laue backscattering X-ray machine. The resultant sample had a total mass of $\sim$1.6 g and a planar mosaic of about 2°. The plates were mounted on an aluminium sample holder, as shown in Supplementary Fig. 1b. Gadolinium oxide powder and cadmium plates (both Ga and Cd are strong neutron absorbers) were used to mask the excess aluminium.

The YBCO6.6 sample (data in Fig. 1c) was previously measured in refs 23,45. The sample was grown with a top-seed melt texturing method and heat-treated to an underdoped state with $T_c=61\pm2.5$ K. We estimate the doping level to be $p=0.11$ from the $T_c$ versus doping relation in ref. 46.

**Definition of wave vector.** We quote the scattering wave-vector $\mathbf{Q}=H\mathbf{a}^*+K\mathbf{b}^*+L\mathbf{c}^*$ as ($H$, $K$, $L$) in reciprocal lattice units (r.l.u.), where $a^*=b^*=1.62$ Å$^{-1}$ and $c^*=0.66$ Å$^{-1}$ are the room-temperature magnitudes. The reduced two-dimensional wave vector is $\mathbf{q}=h\mathbf{a}^*+k\mathbf{b}^*$ and $\mathbf{q}_{AF}=(1/2,1/2)$ r.l.u..

**Time-of-flight measurements.** The time-of-flight measurements were performed with the ARCS spectrometer at the Spallation Neutron Source, Oak Ridge National Laboratory. The HgUD71 sample was mounted such that the incoming beam was parallel to the $c$ axis of the sample. This means that for a particular in-plane wave vector ($H$, $K$), the out-of-plane component $L$ depends on the energy transfer. Two measurement configurations were used: incident energies $E_i=70$ and 130 meV, with Fermi-chopper frequencies of 420 and 600 Hz, respectively. The energy and momentum resolutions as a function of the energy transfer are presented in Supplementary Fig. 2. The out-of-plane wave-vector varies monotonically from $L\approx2$–8 between $\omega=10$–100 meV. As described in Supplementary Notes 1 and 2, the data are processed to isolate the AF fluctuations, and normalized by the magnetic form factor and Bose population factor to obtain $\chi''(\mathbf{Q},\omega)$. Inherent to our analysis is the assumption that the magnetic response arises from the quintessential $CuO_2$ planes and hence is quasi-two-dimensional, and that corrections for the $L$ dependence can be made by accounting for the Cu magnetic form factor.

**Triple-axis measurements with unpolarized neutrons.** Measurements on HgUD71 were performed with the HB3 spectrometer at the High-Flux Isotope Reactor at Oak Ridge National Laboratory (Fig. 1b). Measurements on YBCO6.6 (Fig. 1c) were performed with the 2T spectrometer at the Laboratoire Léon Brillouin (LLB, France) on the same twinned YBCO crystal ($T_c=61\pm2.5$ K, $p=0.11$) used to measure the $\mathbf{q}=0$ magnetic order in ref. 23. Pyrolytic graphite (PG) monochromators and analysers were used to select incident and final neutron energies, and PG filters were used to suppress contamination due to higher harmonics. The samples were mounted in the ($HHL$) scattering plane. Measurements were performed with fixed final energies $E_f=14.7$ meV (HB3), and 35 meV (2T). On HB3, the horizontal collimation configuration was 48′-80′-sample-80′-120′. On 2T, no collimation was used, since vertical and horizontal focusing was employed at the monochromator. The typical energy resolution in the $\omega=50$–60 meV energy transfer range was $\sim$8 meV.

## References


1. Fujita, H. *et al.* Progress in neutron scattering studies of spin excitations in high-$T_c$ cuprates. *J. Phys. Soc. Jpn.* **81,** 011007 (2012).
2. Sidis, Y. *et al.* Inelastic neutron scattering study of spin excitations in the superconducting state of high temperature superconductors. *C. R. Phys.* **8,** 745–762 (2007).
3. Lipscombe, O. J., Vignolle, B., Perring, T. G., Frost, C. D. & Hayden, S. M. Emergence of coherent magnetic excitations in the high temperature underdoped superconductor $La_{2-x}Sr_xCuO_4$ at low temperatures. *Phys. Rev. Lett.* **102,** 167002 (2009).
4. Kivelson, S. A. *et al.* How to detect fluctuating stripes in the high-temperature superconductors. *Rev. of Mod. Phys.* **75,** 1201–1241 (2003).
5. Norman, M. R. Magnetic collective mode dispersion in high-temperature superconductors. *Phys. Rev. B* **63,** 092509 (2001).
6. Dai, P. *et al.* The magnetic excitation spectrum and thermodynamics of high-$T_c$ superconductors. *Science* **284,** 1344–1347 (1999).
7. Hinkov, V. *et al.* Spin dynamics in the pseudogap state of a high-temperature superconductor. *Nat. Phys.* **3,** 780–785 (2007).
8. Hinkov, V. *et al.* Neutron scattering study and analytical description of the spin excitation spectrum of twin-freeYBa2Cu3O6.6, Preprint at http://arxiv.org/abs/1006.3278 (2010).
9. Scalapino, D. J. A common thread: the pairing interaction for unconventional superconductors. *Rev. Mod. Phys.* **84,** 1383–1417 (2012).
10. Metlitski, M. A. & Sachdev, S. Quantum phase transitions of metals in two spatial dimensions. II. Spin density wave order. *Phys. Rev. B* **82,** 075128 (2010).
11. Efetov, K. B., Meier, H. & Pépin, C. Pseudogap state near a quantum critical point. *Nat. Phys.* **9,** 442–446 (2013).
12. Wang, Y. & Chubukov, A.V. Charge order and loop currents in hole-doped cuprates. *Phys. Rev. B* **90,** 035149 (2014).
13. Allais, A., Bauer, J. & Sachdev, S. Bond instability in a correlated two-dimensional metal. *Phys. Rev. B* **90,** 155114 (2014).
14. Atkinson, W. A., Kampf, A. P. & Bulut, S. Charge order in the pseudogap phase of the cuprate superconductors. *New J. Phys.* **17,** 013025 (2015).
15. Tabis, W. *et al.* Connection between charge-density-wave order and charge transport in the cuprate superconductors. *Nat. Commun.* **5,** 5875 (2014).
16. Li, Y. *et al.* Unusual magnetic order in the pseudogap region of the superconductor $HgBa_2CuO_{4+\delta}$. *Nature* **455,** 372–375 (2008).
17. Li, Y. *et al.* Magnetic order in the pseudogap phase of $HgBa_2CuO_{4+\delta}$ studied by spin-polarized neutron diffraction. *Phys. Rev. B* **84,** 224508 (2011).
18. Eisaki, H. *et al.* Effect of chemical inhomogeneity in bismuth-based copper-oxide superconductors. *Phys. Rev. B* **69,** 064512 (2004).
19. Chan, M. K. *et al.* Validity of Kohler's rule in the pseudogap phase of the cuprate superconductors. *Phys. Rev. Lett.* **113,** 177005 (2014).

20. Barišić, N. *et al.* Universal sheet resistance and revised phase diagram of the cuprate high-temperature superconductors. *Proc. Natl Acad. Sci. USA* **110,** 12235–12240 (2013).
21. Mirzaei, S. I. *et al.* Spectroscopic evidence for Fermi liquid-like energy and temperature dependence of the relaxation rate in the pseudogap phase of the cuprates. *Proc. Natl Acad. Sci. USA* **110,** 5774–5778 (2013).
22. Barišić, N. *et al.* Universal quantum oscillations in the underdoped cuprate superconductors. *Nat. Phys.* **9,** 761–764 (2013).
23. Fauqué, B. *et al.* Magnetic order in the pseudogap phase of high $T_c$ superconductors. *Phys. Rev. Lett.* **96,** 197001 (2006).
24. Balédent, V. *et al.* Evidence for competing magnetic instabilities in underdoped $YBa_2Cu_3O_{6+x}$. *Phys. Rev. B* **83,** 104504 (2011).
25. Blanco-Canosa, S. *et al.* Resonant X-ray scattering study of charge density wave correlations in $YBa_2Cu_3O_{6+x}$. *Phys. Rev. B* **90,** 054513 (2014).
26. Ghiringhelli, G. *et al.* Long-range incommensurate charge fluctuations in $(Y,Nd)Ba_2Cu_3O_{6+x}$. *Science* **337,** 821–825 (2012).
27. Chang, J. *et al.* Direct observation of competition between superconductivity and charge density wave order in $YBa_2Cu_3O_{6.67}$. *Nat. Phys.* **8,** 871–876 (2012).
28. Haug, D. *et al.* Neutron scattering study of the magnetic phase diagram of underdoped $YBa_2Cu_3O_{6+x}$. *New J. Phys.* **12,** 105006 (2010).
29. Boebinger, G. S. *et al.* Insulator-to-metal crossover in the normal state of $La_{2-x}Sr_xCuO_4$ near optimum doping. *Phys. Rev. Lett.* **77,** 5471 (1996).
30. Sebastian, S. E. *et al.* Metal-insulator quantum critical point beneath the high $T_c$ superconducting dome. *Proc. Natl Acad. Sci. USA* **107,** 6175–6179 (2009).
31. Yu, G. *et al.* Magnetic resonance in the model high-temperature superconductor $HgBa_2CuO_{4+\delta}$. *Phys. Rev. B* **81,** 064518 (2010).
32. Yu, G., Li, Y., Motoyama, E. M. & Greven, M. A universal relationship between magnetic resonance and superconducting gap in unconventional superconductors. *Nat. Phys.* **5,** 873–875 (2009).
33. Li, Y. *et al.* Doping-dependent photon scattering resonance in the model high-temperature superconductor $HgBa_2CuO_{4+\delta}$ revealed by Raman scattering and optical ellipsometry. *Phys. Rev. Lett.* **111,** 187001 (2013).
34. Vishik, I. M. *et al.* Angle-resolved photoemission study of $HgBa_2CuO_{4+\delta}$. *Phys. Rev. B* **89,** 195141 (2014).
35. Le Tacon, M. *et al.* Two energy scales and two distinct quasiparticle dynamics in the superconducting state of underdoped cuprates. *Nat. Phys.* **2,** 537–543 (2006).
36. Norman, M. R., Pines, D. & Kallin, C. The pseudogap: friend or foe of high $T_c$? *Adv. Phys.* **54,** 715–733 (2007).
37. Varma, C. M. Theory of the pseudogap state of the cuprates. *Phys. Rev. B* **73,** 155113 (2006).
38. Das, T. In-plane anisotropy in spin-excitation spectra originating from chain states in $YBa_2Cu_3O_{6+y}$. *Phys. Rev. B* **85,** 144510 (2012).
39. Alldredge, J. W., Fujita, K., Eisaki, H., Uchida, S. & McElroy, K. Three-component electronic structure of the cuprates derived from spectroscopic-imaging scanning tunneling microscopy. *Phys. Rev. B* **85,** 174501 (2012).
40. Enoki, M. *et al.* Spin-stripe density varies linearly with the hole content in single-layer $Bi_{2+x}Sr_{2-x}CuO_{6+y}$ cuprate superconductors. *Phys. Rev. Lett.* **110,** 017004 (2013).
41. Fauqué, B. *et al.* Dispersion of the odd magnetic resonant mode in near-optimally doped $Bi_2Sr_2CaCu_2O_{8+\delta}$. *Phys. Rev. B* **76,** 214512 (2007).
42. Zhao, X. *et al.* Crystal growth and characterization of the model high-temperature superconductor $HgBa_2CuO_{4+\delta}$. *Adv. Mater.* **18,** 3243–3247 (2006).
43. Barišić, N. *et al.* Demonstrating the model nature of the high-temperature superconductor $HgBa_2CuO_{4+\delta}$. *Phys. Rev. B* **78,** 054518 (2008).
44. Yamamoto, A., Hu, W.-Z. & Tajima, S. Thermoelectric power and resistivity of $HgBa_2CuO_{4+\delta}$ over a wide doping range. *Phys. Rev. B* **63,** 024504 (2000).
45. Pintschovius, L. *et al.* Pronounced in-plane anisotropy of phonon anomalies in $YBa_2Cu_3O_{6.6}$. *Phys. Rev. Lett.* **89,** 037001 (2002).
46. Liang, R., Bonn, D. A. & Hardy, W. N. Evaluation of $CuO_2$ plane hole doping in $YBa_2Cu_3O_{6+x}$ single crystals. *Phys. Rev. B* **73,** 180505 (2006).


## Acknowledgements

We acknowledge fruitful discussions with Yuan Li and Chandra Varma. We thank A. Kreyssig and A.I. Goldman, C.L. Broholm and S. Koopayeh for assistance with crystal alignment work partially performed at Ames Laboratory and at the IQM at Johns Hopkins University. The work at the University of Minnesota was supported by the US Department of Energy, Office of Basic Energy Sciences, under Award No. DE-SC0006858. Research conducted at ORNL's High-Flux Isotope Reactor and Spallation Neutron Source was sponsored by the Scientific User Facilities Division, Office of Basic Energy Sciences, the US Department of Energy. M.K.C. is supported by funds from the US Department of Energy BES grant no. LANLF100. Work at the IQM was supported by the US Department of Energy, Office of Basic Energy Sciences, Division of Materials Sciences and Engineering under award DE-FG02-08ER46544. We also acknowledge financial support at LLB from the projects UNESCOS (contract ANR-14-CE05-0007) and NirvAna (contract ANR-14-OHRI-0010) of the ANR.

## Author contributions

M.K.C., L.M.-T. and Y.T. performed the neutron-scattering experiments. M.K.C., C.J.D, Y.G., M.J.V., G.Y. and X.Z. performed crystal growth, characterization and co-alignment. A.D.C, J.T.P., Y.S., P.S., P.B. and D.L.A. were local contacts for the neutron-scattering experiments. M.K.C., Y.S., P.B. and M.G. wrote the manuscript with input from all authors.

## Additional information

**Supplementary Information** accompanies this paper at http://www.nature.com/naturecommunications

**Competing financial interests:** The authors declare no competing financial interests.

**Reprints and permission** information is available online at http://npg.nature.com/reprintsandpermissions/

**How to cite this article:** Chan, M. K. *et al.* Commensurate antiferromagnetic excitations as a signature of the pseudogap in the tetragonal high-$T_c$ cuprate $HgBa_2CuO_{4+\delta}$. *Nat. Commun.* 7:10819 doi: 10.1038/ncomms10819 (2016).